國 立 交 通 大 學

材 料 科 學 與 工 程 研 究 所

碩 士 論 文

鐵-9 鋁-30 錳-2.5 鉻-0.6 碳合金之相變化

Phase Transformations in an Fe-9Al-30Mn-2.5Cr-0.6C Alloy

研究生　：陳信良

指導教授：劉增豐　教授

朝春光　教授

中 華 民 國 九 十 六 年 七 月

鐵-9 鋁-30 錳-2.5 鉻-0.6 碳合金之相變化

Phase Transformations in an Fe-9Al-30Mn-2.5Cr-0.6C Alloy

研 究 生 ： 陳信良　　Student : Shin-Liang Chen

指導教授 ： 劉增豐博士　　Advisor : Dr. Tzeng-Feng Liu

朝春光博士　　Dr. Chuen-Guang Chao

國 立 交 通 大 學

材 料 科 學 與 工 程 研 究 所

碩 士 論 文

A Thesis

Submitted to Institute of Material Science and Engineering

College of Engineering

National Chiao Tung University

In partial Fulfillment of the Requirements

For the degree of

Master of Science

In

Materials Science and Engineering

July 2007

Hsinchu, Taiwan, R.O.C.

中華民國九十六年七月

誌謝

由衷感謝指導教授 **劉增豐**博士與 **朝春光**博士在學生求學期間的悉心指導與諄諄教誨，尤其在論文上的指導使得學生能順利完成本篇論文的製作。在此，對吾師 **劉增豐**教授與 **朝春光**教授獻上最高的敬意。

研究期間，首先要感謝**段逸軒**學長的提攜，讓我在實驗上能獲得傾力的協助與論文撰寫之指導。另外，感謝**蘇俊瑋**與**林志龍**學長在電子顯微鏡的操作與數據分析上的教導；以及感激**鄭祥誠**、**李堅瑋**、**王承舜**、**楊勝裕**等諸位學長在當我遇到問題時幫忙解惑與生活的協助。同時，感謝**蔡政堯**、**翁瑞陞**、**曾傑享**、**黃世陽**、**郭柏村**、**陳柏至**、**蔡雨霖**、**劉哲郎**、**王浩仰**、**林欣龍**、**黃敬恆**等實驗室歷屆學長弟們，陪伴我一起同歡樂共甘苦。此外，要感謝在中央機械系任教的舅舅 **曾重仁**教授從旁協助我處理生活與實驗上的問題，呂志鵬教授實驗室的**車牧龍**同學、台大材料所表面處理實驗室**李偉任**同學與台大醫工所藥物制放實驗室的**陳德軒**同學時常提供實驗儀器與文獻搜尋的資訊。

最後，將這篇論文謹獻給我最敬愛的父母親、妹妹**玟玲**與妹婿**明伯**、弟弟**信豪**，與諸位死黨好友們，感謝他們的支持與鼓勵，讓我能在安定舒適的環境中順利完成學業。

中文摘要

我們使用掃描式電子顯微鏡(SEM)、穿透式電子顯微鏡(TEM)與 X 光能量散佈分析儀(EDS)，研究鐵-9 鋁-30 錳-2.5 鉻-0.6 碳合金的相變化。

鐵-9 鋁-30 錳-2.5 鉻-0.6 碳合金在淬火狀態下之顯微結構是沃斯田鐵相(γ)與肥粒鐵(α)相的雙相結構。藉由電子繞射技術證實於固溶淬火過程中沒有任何析出物在沃斯田鐵相與肥粒鐵相之中產生。在 650℃的溫度下進行不同時間的時效處理後，在時效處理初期，我們觀察到沃斯田鐵相中並無任何析出，但是在肥粒鐵相的基地中發現生成$D0_3$ 相與$M_{23}C_6$及M_5C_2 兩種碳化物。隨著時效時間的增加，在沃斯田鐵相的基地中生成κ' carbide此碳化物，此外，β-Mn相也在肥粒鐵相的基地中形成。在我們的認知當中，具有單斜結構(monoclinic structure)的M_5C_2碳化物是第一次在鐵鋁錳合金系統中被觀察發現，而且此M_5C_2碳化物與$D0_3$相和β-Mn相共存，這是從未被發現過的情形。此一研究結果與鐵-8.8 鋁-30 錳-6 鉻-1.0 碳合金與鐵-8.8 鋁-30 錳-2.5 鉻合金等文獻的結果有相當大的不同。

Abstract

Phase transformations in an Fe-9Al-30Mn-2.5Cr-0.6C alloy have been examined by means of scanning electron microscopy (SEM), transmission electron microscopy (TEM), and energy-dispersive X-ray spectrometry (EDS).

In the as-quenched condition, the microstructure of the alloy was (austenite + ferrite) dual-phases. No precipitate was found within the ferrite phase and austenite phase in the as-quenched specimen, which was confirmed by the electron diffraction method. When the alloy was aged at 650℃, the phase transformation sequence as the aging time increased was found to be $[\gamma + \alpha] \rightarrow [\gamma + (\alpha + D0_3 + M_{23}C_6 + M_5C_2)] \rightarrow [(\gamma + \kappa'$ carbide) + $(\alpha + D0_3 + \beta\text{-Mn} + M_{23}C_6 + M_5C_2)]$. It is noted that, the monoclinic type M_5C_2 carbide has not been observed by other workers in Fe-Al-Mn alloy systems before. In addition, the coexistence of M_5C_2 carbide, $D0_3$ and β-Mn has also never been reported in the previous literatures. These results are quite different from the previously observations in the Fe-8.8Al-30Mn-6Cr-1.0C alloy and Fe-9.1Al-29.9Mn -2.9Cr alloy.

CONTENT

List of Table

List of Figures

24 hours. (c) BF, (d) and (e) two SADPs taken from the grain marked as “A” in (b). The foil normals are [001] and [011], respectively. ($\underline{hkl}$ = austenite matrix；hkl = κ' carbide). (f) (100) κ' carbide DF. (g) BF, (h) an SADP taken from the ferrite matrix marked as “D” in (g). The foil normal is [110]. (i) and (j) two SADPs taken from the ferrite matrix marked as “B” in (g). The foil normals are [001] and [011], respectively.

Fig.4 (a) an SEM micrograph of the alloy aged at 650℃ for 7 days. (b) SEM, (c)BF, (d) an SADP taken from the austenite matrix marked as A in (a). The foil normal is [001]. ($\underline{hkl}$ = austenite matrix；hkl = κ' carbide). (e) (100) κ' carbide DF. (f) SEM, (g) BF electron micrograph taken from the grain marked as “F” in (a). (h) an SADP taken from the ferrite matrix marked as “$D0_3$” in (f). The foil normal are [011]. (i) and (j) two SADPs taken from the grain marked as “β Mn” in (f). The foil normals are [011] and [$\bar{1}$11], respectively.

INTRODUCTION

In order to develop a new high-strength high-ductility alloy steel, a considerable attention has been concentrated on the development of Fe-Mn-Al-C alloys.[1-9] In this alloy system, manganese and carbon are austenite stabilizers whereas aluminum is a ferrite former. The amount of manganese necessary to produce a face-centered cubic (F.C.C) structure depends on the contents of aluminum and carbon in the alloy. In general, the F.C.C. structure can be stabilized by increasing the contents of manganese and carbon or decreasing the content of aluminum. Therefore, through a proper combination of aluminum, manganese, and carbon, an alloy with a fully austenitic structure can be achieved. After being solution heat-treated and aged at temperatures ranging from 450℃ to 650℃ for moderate times, the austenitic alloy can possess a remarkable combination of strength and ductility, which is attributed to the formation of extremely fine $(Fe,Mn)_3AlC$ carbides (K phase) within the austenite matrix. [1-9] The $(Fe,Mn)_3AlC$ carbide has an order F.C.C. crystal structure which belongs to the $L'1_2$ type. [5]

After prolonged aging within this temperature range, $(Fe,Mn)_3AlC$

carbides were found to precipitate not only coherently within the austenite matrix, but also on the grain boundaries in the form of coarser particles. Besides the precipitation of $(Fe,Mn)_3AlC$ carbides, A13 β-Mn precipitates could also be observed to form on the grain boundaries through a $\gamma \rightarrow \alpha + \beta$-Mn transition. The formation of $(Fe,Mn)_3AlC$ carbides and β-Mn precipitates on the grain boundaries resulted in the embrittlement of the alloy.

In previous studies, it is clear that fully austenitic Fe-Mn-Al-C alloys could possess excellent mechanical properties. However, the corrosion resistance of the austenitic Fe-Mn-Al-C alloys in aqueous environments was not adequate for the applications in industry.[10-13] Since carbon was reported to be detrimental to the corrosion resistance, reducing the carbon content may be an effective way to improve the corrosion resistance of the Fe-Mn-Al-C alloys. However, it was found that with lower C content, the Fe-(24.0-30.0)Mn-(8.9-10.5)%Al-(0.4-0.6)%C alloys consisted of (austenite + ferrite) dual phases.[6 , 14] However, the previous studies have shown that in the dual-phase Fe-Mn-Al-C alloys, in order to improve the corrosion resistance, 3.1~6.2% Cr has been added to the dual-phase Fe-(21.5-27.7)%Mn-(8.8-9.9)%Al-(0.33-0.42)C alloys.[14] Consenquently,

it was found that the addition of Cr could be effective in the improvement of the corrosion resistance of the dual-phase Fe-Mn-Al-C alloys. However, although the corrosion behaviors of the dual-phase Fe-Mn-Al-Cr-C alloys have been studied, information concerning the microstructural development of the dual-phase Fe-Mn-Al-Cr-C alloys is very deficient. Therefore, the purpose of this study is an attempt to examine the phase transformations in the Fe-9%Al-30%Mn-2.5Cr-0.6C alloy.

EXPERIMENTAL PROCEDURE

(A) Alloy preparation :

The alloy, Fe-9wt%Al-30wt%Mn-2.5wt%Cr-0.6wt%C, was prepared in an air induction furnace by using electrolytic iron (99.5%), electrolytic aluminum (99.7%), electrolytic manganese (99.9%), electrolytic chromium (99.9%) and pure carbon powder . After being homogenized at 1250℃ for 48 hours under a protective argon atmosphere, the ingot was hot-forged and cold-rolled to a final thickness of 3.0mm. The sheets were subsequently solution heat-treated at 1050℃ for 2 hours and rapidly quenched into room-temperature water. The aging processes were performed at the temperature of 650℃ for various times in a vacuum furnace and then quenched into water rapidly.

(B)Microstructure observations and diffraction analyses :

The optical microscopy specimens were prepared as the following steps : sectioning, mounting, rough polishing, fine polishing and finally etching with 10% nital. Specimens for electron microscopy

were prepared by means of a double-jet electropolisher with an electrolyte of 30% acetic acid, 60% ethanol and 10% prechloric acid . The polishing temperature was kept in the range from 0℃ to 10℃, and the current density was kept in the range from 3.5 to $4.0x10^4$ A/m^2. Electron microscopy was proformed on JEOL 2000FX scanning transmission electron microscope (STEM) operating at 200kV. This microscope was equipped with a Link ISIS 300 energy-dispersive X-ray spectrometer (EDS) for chemical analysis. In the present study, the elemental analysis was done in the STEM mode on thin films.

Scanning electron microscopy (SEM) samples were prepared similar to STEM sample. SEM was performed on a JEOL 6500FX Field-emission SEM operating at 15kV. The SEM microscope was equipped with an energy-dispersive X-ray spectrometer (EDS) for chemical analyses and distribution. Quantitative analyses of elemental concentrations for Fe , Al , Mn and Cr were made with the aid of a Cliff-Lorimer ratio thin section method.

Results

I. As-quenched microstructure :

Figures 1(a) and 1(b) are two SEM micrographs of the alloy after being solution heat-treated at 1050℃ for 1 hour and then quenched into water. In these figures, the grains with annealing twins (i.e. marked as A) are austenite phase(γ), whereas other grains (i.e. marked as F) are ferrite phase(α). The volume fraction of the ferrite phase is about 30% , as determined by a point-counting technique. Figures 1(c) and 1(d) show two different selected-area diffraction patterns (SADPs) taken from a ferrite grain marked as F in Figure 1(b), exhibiting the reflection spots of the disordered body-centered cubic (B.C.C.) structure.[14] Figures 1(e) and (f) are two SADPs taken from an austenite grain marked as A in Figure 1(b), showing that the grain has a disordered face-centered cubic (F.C.C.) structure. [14] It is seen in figures 1(d) and 1(f) that in addition to the reflection spots corresponding to the ferrite (α) and austenite phase (γ), no precipitate was found within the ferrite phase and austenite phase in the as-quenched specimen, which was confirmed by the electron diffraction method. These results show that the as-quenched microstructure of the

alloy are (austenite + ferrite) dual-phases.

II. Aged microstructures :

Figures 2(a) through 2(c) show three SEM micrographs of the alloy aged at 650℃ for 30 minutes and then quenched into water rapidly. It reveals two distinctive regions (marked as “A” and “F”, respectively). Figure 2(d) is an SADP taken from an area marked as “A”. The zone axis is [111]. It is clearly seen that these reflection spots are of single austenite phase. Figure 2(e) is a bright-field (BF) electron micrograph taken from an area marked as “F”, revealing that some precipitates were formed within the matrix. Figure 2(f), an SADP taken from the ferrite matrix, shows that in addition to the reflection spots correspond to the ferrite phase, the diffraction pattern also consists of the superlattice reflection spots of the $D0_3$ phase.[15 . 16] Figure 2(g) is a $(\bar{1}11)$ $D0_3$ dark-field (DF) electron micrograph, showing a high density of extremely fine $D0_3$ precipitates were formed within the ferrite matrix.

Figure 2(h) is a BF electron micrograph taken from the granular-like precipitate on the grain boundary in Figure 2(c). Figure 2(i) and Figure 2(j) are two SADPs from the granular-like precipitate in Figure 2(h).

From the camera length and the measurements of angles as well as d-spacings of diffraction spots, the crystal structure of the precipitate was determined to be an F.C.C. structure with a lattice parameter a = 1.073nm, which is consistent with that $M_{23}C_6$.[17] ("M" stands for the metal atoms, i.e. Fe, Mn, Al, or Cr elements substituting Fe in its lattice sites, in appropriate proportions). Figure 2(k) is a BF electron micrograph, showing that fine sheet-like precipitates were formed within the ferrite matrix as Figure 2(c). Figures 2(l) through 2(q) demonstrate six different SADPs taken from the precipitate marked as P_2 in Figure 2(k). These SADPs were obtained by tilting the specimen about some specific reflections. Based on these SADPs, an attempt was made to determine the structure of the precipitate. However, it could not be indexed completely by any known phases reported in Fe-Mn-Al, Fe-Mn-Al-Cr, and Fe-Mn-Al -Cr-C alloy systems. [1-18]

All SADPs in Figures 2(l) through 2(q) belong to the sheet-like precipitates and can be used to carry out an unambiguous identification about the precipitates. Table I contains the interplanar spacings of the precipitate's structure, which were measured directly from the SADPs in Figures 2(l) through 2(q). The measured angles among the reciprocal

lattice vectors are listed in Table II. Using these measured values of interplanar spacings and angles, the crystal structure of the precipitate phase could be determined to be monoclinic with lattice parameters a = 1.2270 nm, b = 0.4555 nm, c = 0.5058 nm, β= 98.70 deg.

By means of the above lattice parameters, the interplanar spacing and the angles between the chosen reciprocal reflections can be calculated using the following equations:

Interplannar spacing of the (hkl) plane

$$\frac{1}{d^2}=\frac{1}{a^2}\frac{h^2}{\sin^2\beta}+\frac{1}{b^2}k^2+\frac{1}{c^2}\frac{l^2}{\sin^2\beta}-\frac{2hl\cos\beta}{ac\sin^2\beta}$$

Angleψ between ($h_1k_1l_1$) and ($h_2k_2l_2$)

$$\cos\varphi=\frac{\frac{1}{a^2}h_1h_2+\frac{1}{b^2}k_1k_2\sin^2\beta+\frac{1}{c^2}l_1l_2-\frac{1}{ac}(l_1h_2+l_2h_1)\cos\beta}{\sqrt{(\frac{1}{a^2}h_1^2+\frac{1}{b^2}k_1^2\sin^2\beta+\frac{1}{c^2}l_1^2-\frac{2h_1l_1}{ac}\cos\beta)}\times\sqrt{(\frac{1}{a^2}h_2^2+\frac{1}{b^2}k_2^2\sin^2\beta+\frac{1}{c^2}l_2^2-\frac{2h_2l_2}{ac}\cos\beta)}}$$

The calculated interplanar spacings and angles are also listed in Table I and Table II for comparison. It is seen in Table I and Table II that

the measured values are quite consistent with those obtained by calculation. Based on this result, therefore, the diffraction patterns of the precipitate phase in Figures 2(l) through 2(q) could all be indexed. The zone axes of the precipitate phase in Figures 2(l) through 2(q) are $[\bar{1}10]$, $[\bar{2}10]$, $[\bar{1}10]$, $[10\bar{1}]$, $[2\bar{1}\bar{2}]$, and $[2\bar{2}1]$, respectively. This result is similar to the Hägg-carbide found by other workers in 316L-type austenitic stainless steel.[18, 19] Based on above analyses, we suggest that the structure of the precipitate is the M_5C_2 carbide (χ-carbide , Hägg carbide). It is worthwhile to be noted here that the M_5C_2 carbide has never been found in Fe-Mn-Al, Fe-Mn-Al-Cr, and Fe-Mn-Al-Cr-C alloy systems before. Based on the above observations, it is concluded that the microstructure of the alloy aged at 650℃ for 30 minutes was a mixute of ($\gamma + D0_3 + M_{23}C_6 + M_5C_2$) phases.

Figures 3(a) and 3(b) show two SEM micrograph of the alloy aged at 650℃ for 24 hours and then quenched into water rapidly. It reveals fine precipitates with a modulated structure were observed within the austenite matrix, as illustrated in Figure 3(c) which is a BF electron micrograph taken from the area marked as A in Figure 3(b). Figures 3(d) and (e) demonstrate two different SADPs taken from the mixed region of

austenite matrix and fine precipitates. The zone axes are [001] and [011], respectively. In addition to the spots corresponding to the austenite matrix, the diffraction patterns also consist of small superlattice spots of 100, 110, 111, etc. caused by the presence of fine precipitates. Compared to the previous studies in the Fe-Mn-Al-C alloy[07], it is clear that the fine precipitates are $(Fe,Mn)_3AlC$ carbide (κ' carbide) having an $L'1_2$ - type structure. Figure 3(f), a DF electron micrograph obtained by use of the 100 superlattice reflection in [001] zone, reveals that the $(Fe,Mn)_3AlC$ carbide were formed along <100> directions. This result is consistent with the appearance of long streaks along <100> reciprocal lattice directions in the diffraction patterns. On the basis of the above observations, it is concluded that the microstructure was the austenite phase containing fine κ' carbides.

Figure 3(g), a BF electron micrograph taken from the ferrire matrix marked as F in Figure 3(b), shows a complex phase transition has occurred within the ferrite matrix. Analyses of the area marked as D showed that the microstructure of the area was also $D0_3$, as shown in Figure 3(h). Figures 3(i) and 3(j) show two SADPs taken from the precipitate marked as B in Figure 3(g). From the camera length and the

measurements of angles as well as d-spacings of diffraction spots, the crystal structure of the precipitate was determined to be a simple cubic (S.C.) structure with a lattice parameter a = 0.632 nm, which is consistent with that of the β-Mn. [9] Based on the above observations, it could be concluded that the microstructure of the alloy aged at 650℃ for 24 hours was a mixute of (γ + κ' carbide + $D0_3$ + β-Mn + $M_{23}C_6$ + M_5C_2) phases.

Figure 4(a) shows an SEM micrograph of the alloy aged at 650℃ for 7 days and then quenched into water rapidly. Figures 4(b) and 4(c) are SEM and BF electron micrograph taken from the austenite matrix marked as A in Figure 4(a), respectively. Figure 4(d), an SADP taken from the austenite matrix, indicates that coarse κ' carbide having an $L'1_2$ type structure were formed within the austenite matrix. Figure 4(e) is a (100) κ' carbide DF electron micrograph, this feature is similar to that observed in the alloy aged at 650℃ for 24 hours.

Figures 4(f) and (g) are SEM and BF electron micrographs taken from the ferrite matrix marked as F in Figure 4(a), respectively. SEM and TEM examinations of the specimens indicated that the (α + β Mn + $M_{23}C_6$ + M_5C_2) phases were preserved up to 7 days. However, the morphology of the β-Mn precipitates was changed from plate-like to

irregular shape. Figure 4(h), an SADP taken from the area marked as D in Figure 4(g), shows that the reflection spots belong to the $D0_3$ phase. Figures 4(i) and (j) show two SADPs taken from the area marked as B in Figure 4(g). These figures indicated that the reflection spots are of the β-Mn precipitates. Based on the above observations, it could be concluded that the microstructure of present alloy in the equilibrium stage at 650℃ was a mixture of (γ + κ' carbide + $D0_3$ + β-Mn + $M_{23}C_6$ + M_5C_2) phases.

The phase transformation sequence occurred in the Fe-30Mn-8.8Al-2.5Cr-0.6C alloy with increasing the aging time was found to be [γ + α] → [γ + ($D0_3$ + $M_{23}C_6$ + M_5C_2)] → [(γ + κ' carbide) + ($D0_3$ + β-Mn + $M_{23}C_6$ + M_5C_2)].

Discussion

Based on the above experimental results, some discussions are appropriate. When the alloy was aged at 650℃ as the aging time increased, the phase transformation sequence was found to be [γ + α] → [γ + ($D0_3$ + $M_{23}C_6$ + M_5C_2)] → [(γ + κ' carbide) + ($D0_3$ + β-Mn + $M_{23}C_6$ + M_5C_2)]. This result is quite different from that reported by other workers in the Fe-Al-Mn-Cr-C alloys.[20-23]

To our knowledge, M_5C_2 carbide has not been observed in the Fe-Al-Mn alloy systems before. In addition, the coexistence of M_5C_2 carbide (Hägg carbide), $D0_3$ and β-Mn has also never been reported in the previous literatures. In ferritic steels, Dirand and Alqier have observed Fe_5C_2 as part of a transformation sequence, which leads from martensite to a phase equilibrium of ferrite (α) and cementite (θ-Fe_3C) in 1983.[24] In the sequently, Fe_5C_2 forms from η-Fe_2C and subsequently decomposes into θ-Fe_3C. Furthermore, F. Ernst et al. [18,19] have reported that the M_5C_2 carbide was presented in the 316-type austenitic stainless steels by using low temperature (470℃) gas-phase carburization treatment. In their work, it is believed that the excess vacancies and the dislocations play a very

important role in the formation of M_5C_2 carbide.

In this present study, it is well-known that the solubility of both the carbon and equilibrium vacancies within ferrite matrix at 1050℃ are more than those at room temperature. When the alloy was solution heat-treated at 1050℃ for 1 hour and then quenched into water, a lot of excess vacancies and carbon atoms might appear in the ferrite region. Thus, it is reasonable to suggest that the M_5C_2 carbide could be formed within the ferrite matrix in the early stage of aged process at 650℃.

In order to clarify the apparent difference, an STEM-EDS study was undertaken. The average concentrations of the alloying elements were obtained by analyzing at least ten different EDS spectra of each phase. EDS with a thick-window detector is limited to detect the elements of atomic number of 11 or above; therefore, carbon cannot be examined by this method. The results are summarized in Table III. It is clearly seen in Table III that the concentrations of the aluminum in the M_5C_2 carbides and $M_{23}C_6$ carbides are much less than that in α phase, and reverse result is obtained for the concentrations of the manganese and chromium. In the precious studies,[15] it is known that the higher aluminum content in the Fe-Mn-Al alloys could enhance the formation of the $D0_3$ phase.

According to Table III, the aluminum content in the M_5C_2 carbides and $M_{23}C_6$ carbides are much lower than that in present alloy. Therefore, it is reasonable to believe that along with the precipitations of the M_5C_2 carbides and $M_{23}C_6$ carbides, the surrounding ferrite phase would be enriched aluminum content. The ferrite phase in the vicinity of the M_5C_2 carbides and $M_{23}C_6$ carbides would transform into the $D0_3$ phase.

With increasing the aging time at the same temperature, it is seen that the manganese content in $D0_3$ phase was noticeably lowered. This indicates that along with the formation of $D0_3$ phase, the region surrounding $D0_3$ phase would be enriched in manganese. The enrichment of manganese content would enhance the formation of Mn-enriched β-Mn precipitates at the region continuous to the $D0_3$ phase. Furthermore, the area of austenite phase adjacent to the $D0_3$ / γ grain boundary would enhance the formation of κ' carbides.

With increasing the aging time from 24 hours to 7 days, SEM and TEM examinations of the specimen indicated that the ($D0_3$ + β Mn + $M_{23}C_6$ + M_5C_2) phases were preserved up to 7 days. However, the morphology of the β-Mn precipitates was changed from plate-like to irregular shape. It could be concluded that the microstructure of present

alloy in the equilibrium stage at 650℃ was a mixture of (γ + κ' carbide + $D0_3$ + β-Mn + $M_{23}C_6$ + M_5C_2) phases.

Conclusions

The phase transformations in the Fe-9Al-30Mn-2.5Cr-0.6C alloy have been investigated in the present study.

(1) In the as-quenched condition, the microstructure of the alloy was (austenite + ferrite) dual-phases, no precipitates were found within the ferrite phase and austenite phase in the matrix. which was confirmed by the electron diffraction method.

(2) The phase transformation sequence occurred within the alloy with increasing aging time was found to be [$\gamma + \alpha$] → [$\gamma + (D0_3 + M_{23}C_6 + M_5C_2)$] → [($\gamma$ + κ' carbide) + ($D0_3$ + β-Mn + $M_{23}C_6$ + M_5C_2)].

(3) The M_5C_2 carbide formation in Fe-Mn-Al alloy systems has not been observed before. In addition, the coexistence of M_5C_2 carbide, $D0_3$ and β-Mn has also never been reported in the previous literatures.

(4) The crystal structure of the M_5C_2 carbide was determined to be monoclinic with lattice parameters a = 1.2270 nm, b = 0.4555 nm, c = 0.5058 nm, β= 98.70 deg.

REFERENCES

1. S.K. Banerji : Met. Prog., p.59, Apr., 1978
2. R. Wang and F.H. Beck : Met. Prog., p.72, Mar., 1983
3. H.W. Leavenworth, Jr. and J.C. Benz : J. Met., p.36, Mar., 1985
4. W.K. Choo and D.G. Kim : Metall. Trans. A, p.5, vol.16A, 1985
5. W.K. Choo and D.G. Kim : Metall. Trans. A, p.759, vol.18A, 1987
6. T.F. Liu, J.S. Chou, and C.C. Wu : Metall. Trans. A, p.1891, vol.21A, 1990
7. C.C. Wu, J.S. Chou, and T.F. Liu : Metall. Trans. A, p.2265, vol.22A, 1991
8. C.N. Wang, C.Y. Chao, and T.F. Liu : Scripta. p.109, vol.28, 1993
9. C.N. Wang, C.Y. Chao, and T.F. Liu : Scripta. p.263, vol.28, 1993
10. C.J. Altstetter, A.P. Bentley, J.W. Fourie, A.N. Kirkbride : Mater. Sci. Eng., p.82, vol.13, 1986
11. T. Wen, B. Jing, T. Ju : J. Mater. Sci., p.3517, vol.22, 1987
12. S.T. Shin, C.Y. Tai, T.P. Perng : Corrosion p.130, vol.49, 1993
13. M. Ruscak, T.P. Perng : Corrosion p.738, vol.51, 1995
14. W.C. Cheng, H.Y. Lin : Mater. Sci. Eng. A, p.426, vol.323, 2002
15. T.F. Liu, and C.M. Wan : Scripta, p.19, vol.6, 1985

16. T.F. Liu, and C.M. Wan : Scripta, p.19, vol.6, 1986
17. T.F. Liu, S.W. Peng, Y.L. Lin, and C.C. Wu : Metall. Trans. A, p.567 vol.21A, 1990
18. F. Ernst, Y. Cao, and G.M. Michal : Acta Mater., p.1469, vol.52, 2004
19. F. Ernst, Y. Cao, G.M. Michal, and A.H. Heuer : Acta Mater., p.1895, vol.55, 2007
20. Y.S. Zhang, X.M. Zhu, M. Liu, R.X. Che : App. Surf. Sci., p.89, vol.222, 2004
21. 蔡國棟，劉增豐 ： 鐵-9.5鋁-30.0錳-5.0鉻-1.5碳合金之相變化. 碩士論文，國立交通大學. 1999年7月
22. 羅亦旋，劉增豐 ： 鐵-8.8鋁-30.0錳-6.0鉻-1.0碳合金之相變化. 碩士論文，國立交通大學. 2000年7月
23. 张晓燕，刘克家，伍玉娇 ： 热处理对Fe-Mn-Al(Cr)-C合金组织的影响. 贵州工业大学学报（自然科学版）, 2001年06期
24. M. Dirand M, L. Afqir : Acta Metall, p.1089, vol.31, 1983
25. C. Hammerl, A. Königer, B. Rauschenbach : J. Mater. Res., p.2614, vol.13, 1998
26. H.I. Faraoun, Y.D. Zhang, C. Esling, H. Aourag : J. App. Phys., vol.99, 2006

Table I. The interplanar spacings of the M_5C_2 phase :

Indexed plane	Observed d spacing (nm)	Calculated d spacing (nm)
001	0.5035	0.5035
101	0.4394	0.4339
110 , $\bar{1}10$	0.4267	0.4267
201	0.3599	0.3599
$\bar{1}11$	0.3342	0.3352
111 , $1\bar{1}1$	0.3166	0.3166
$\bar{1}20$	0.2277	0.2239
012	0.2125	0.2203
202	0.2225	0.2202
$\bar{1}21$	0.2066	0.2069
221	0.1925	0.1925
302	0.2017	0.1997
312	0.1835	0.1829
412	0.1607	0.1674

Table II. Angles among some reciprocal vectors of the M_5C_2 phase :

Two desired reciprocal vectors		Observed angle (degree)	Calculated angle (degree)
A	(001) and (110)	87.0	87.2
	(111) and (110)	39.0	39.0
B	(001) and ($\bar{1}$ 20)	91.5	91.7
	($\bar{1}$ 21) and ($\bar{1}$ 20)	24.5	24.6
C	(001) and ($\bar{1}$ 10)	93.0	93.3
	($\bar{1}$ 11) and ($\bar{1}$ 10)	42.0	42.2
	(1 $\bar{1}$ 1) and ($\bar{1}$ 10)	141.0	140.6
D	(1 $\bar{1}$ 1) and (111)	87.0	87.2
	(101) and (111)	44	43.6
E	(1 $\bar{1}$ 1) and (110)	121.5	121.3
	(201) and (110)	75.0	75.7
F	(302) and (110)	79.0	79.9
	(412) and (110)	54.5	55.2

Table III. Chemical compositions of the phase revealed by energy-dispersive x-ray spectrometer (EDS)

Heat Treatment	Phase	Chemical Compostion (wt%)			
		Al	Mn	Cr	Fe
as-quenched	γ	8.38	37.59	2.38	Bal.
	α	9.68	33.72	2.75	Bal.
Aged at 650℃ for 30 minutes.	γ	7.72	33.78	2.14	Bal.
	$D0_3$	10.71	20.86	0.11	Bal.
	$M_{23}C_6$	3.41	42.01	21.75	Bal.
	M_5C_2	5.48	29.55	8.32	Bal.
Aged at 650℃ for 24 hours.	γ + κ	10.49	31.93	2.23	Bal.
	$D0_3$	11.47	18.18	0.83	Bal.
	β-Mn	8.63	36.23	1.15	Bal.
	$M_{23}C_6$	1.51	40.64	19.58	Bal.
	M_5C_2	2.51	34.30	10.30	Bal.

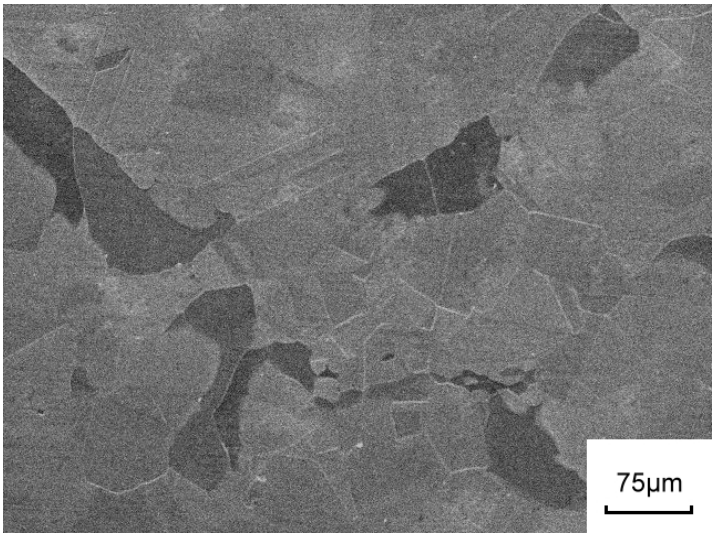

Figure 1(a)

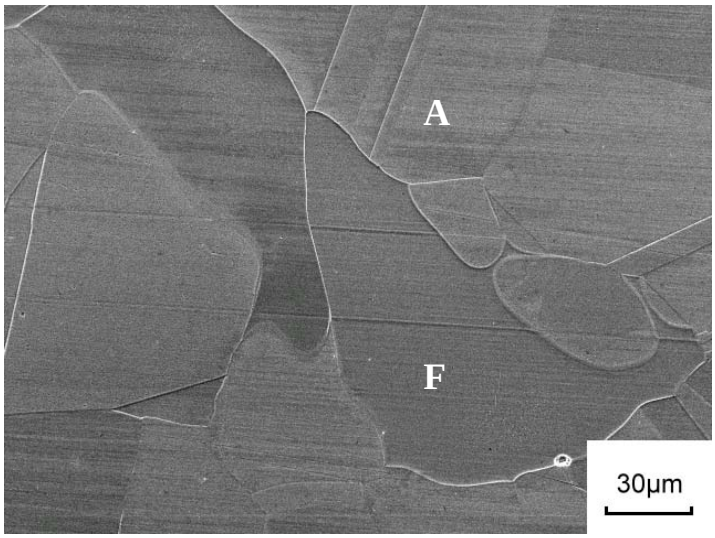

Figure 1(b)

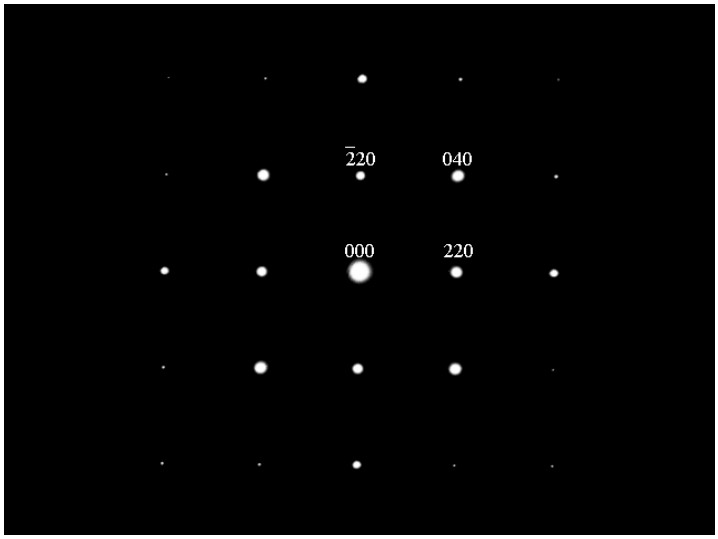

Figure 1(c)

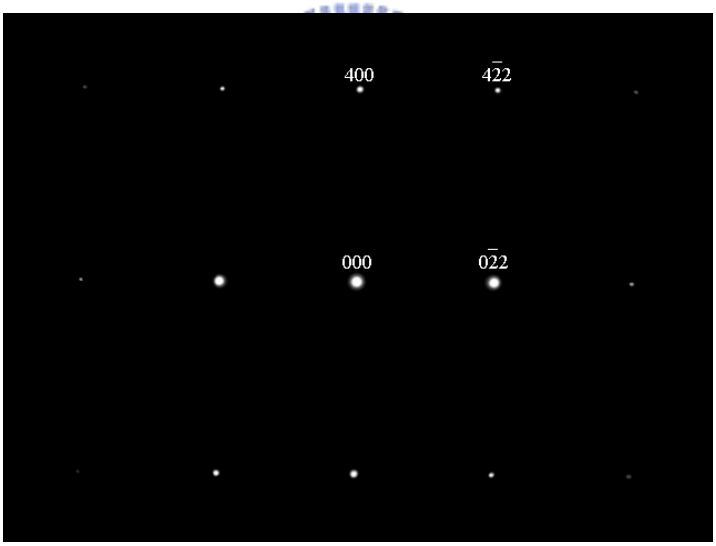

Figure 1(d)

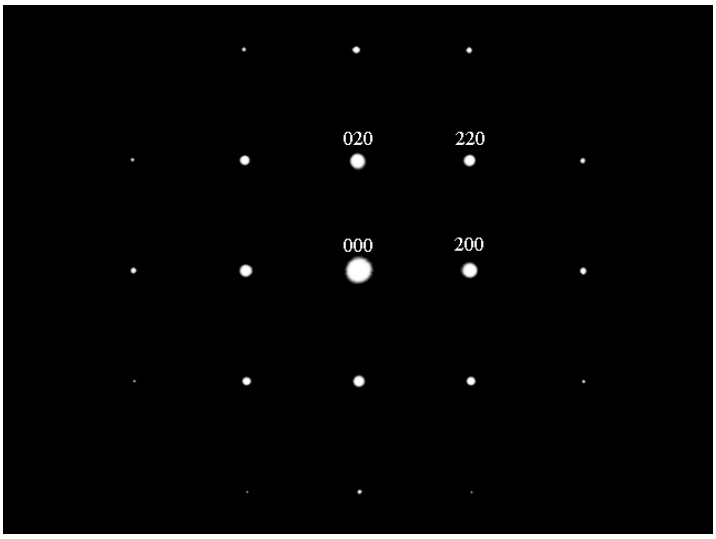

Figure 1(e)

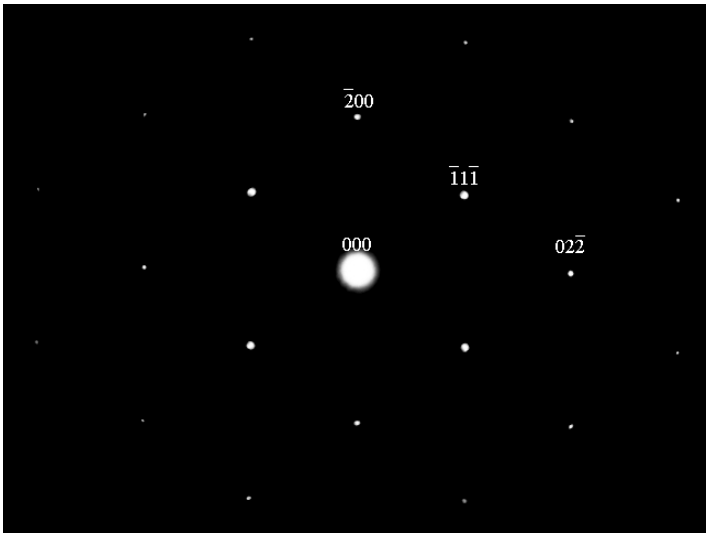

Figure 1(f)

Fig.1 (a) and (b) two SEM micrographs of the as-quenched alloy. (c) and (d) two SADPs taken from the grain marked as “F” in (b). The foil normals are [001] and [011], respectively. (e) and (f) two SADPs taken from the grain marked as “A” in (b). The foil normals are [001] and [011], respectively.

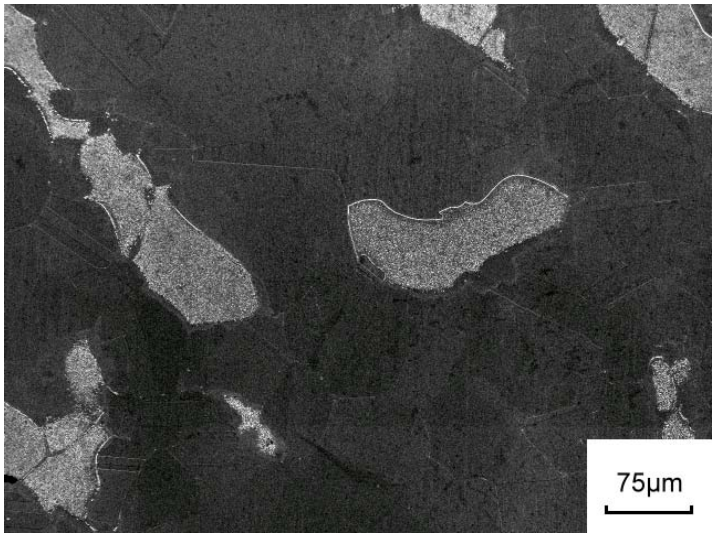

Figure 2(a)

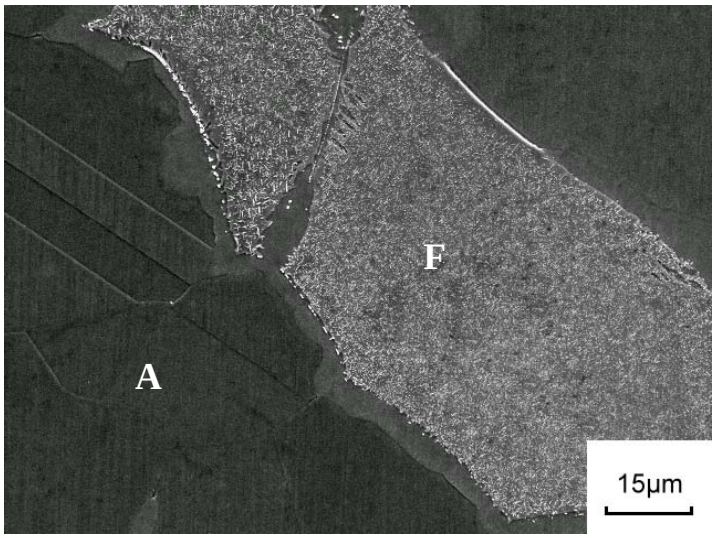

Figure 2(b)

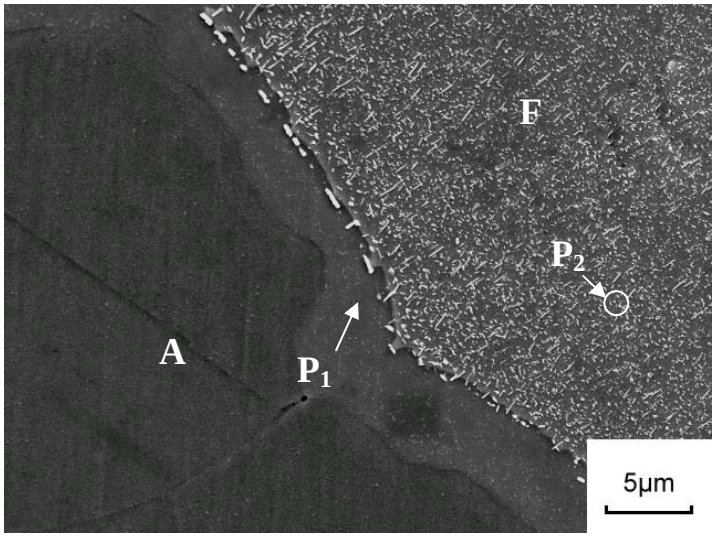

Figure 2(c)

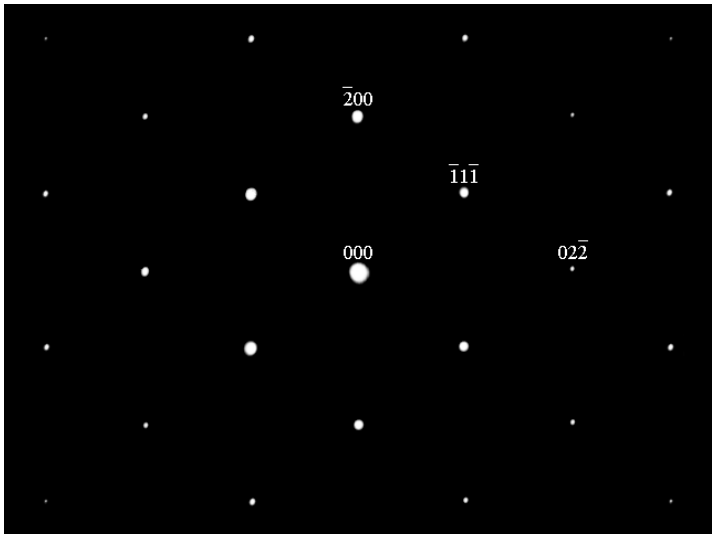

Figure 2(d)

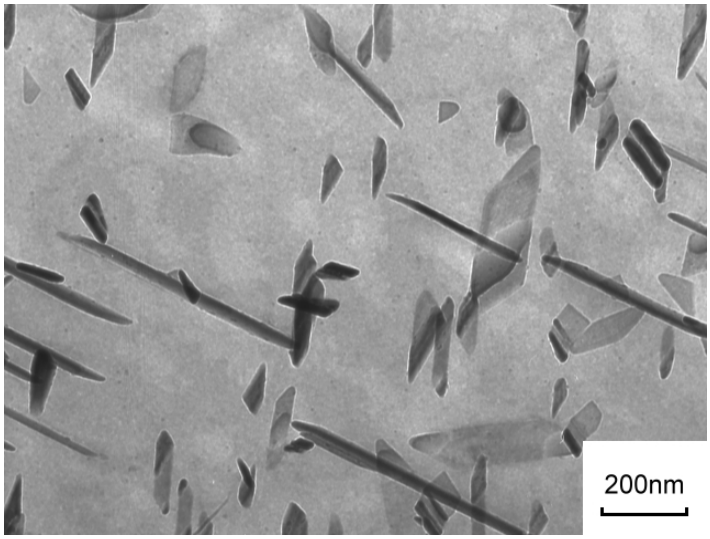

Figure 2(e)

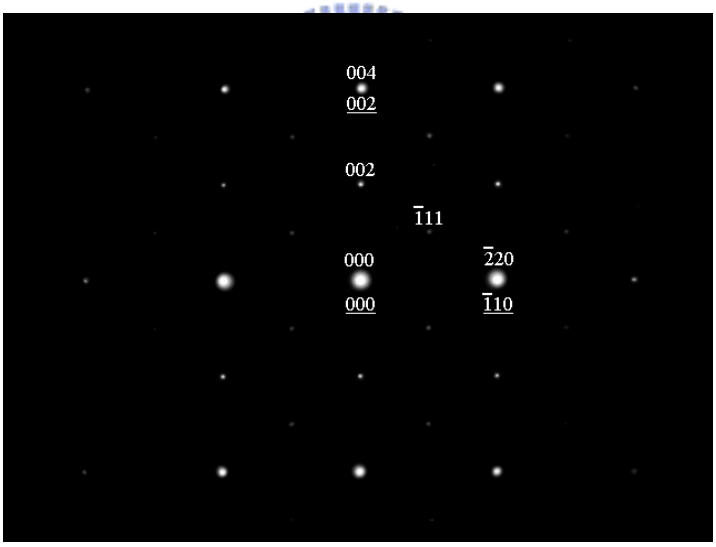

Figure 2(f)

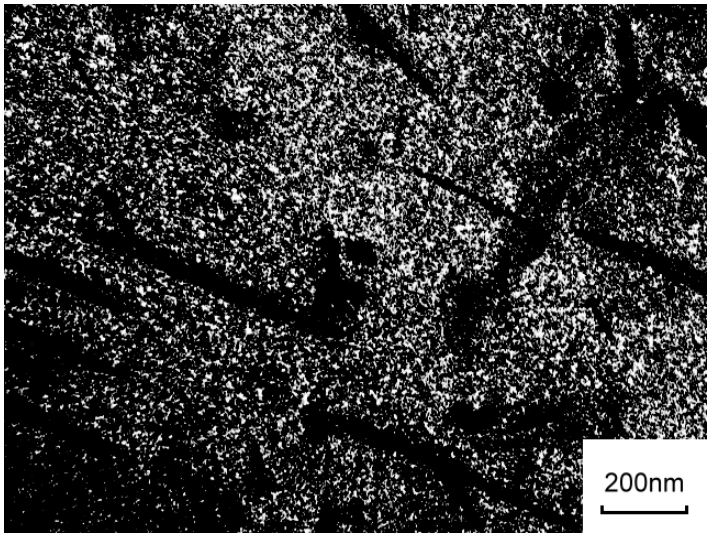

Figure 2(g)

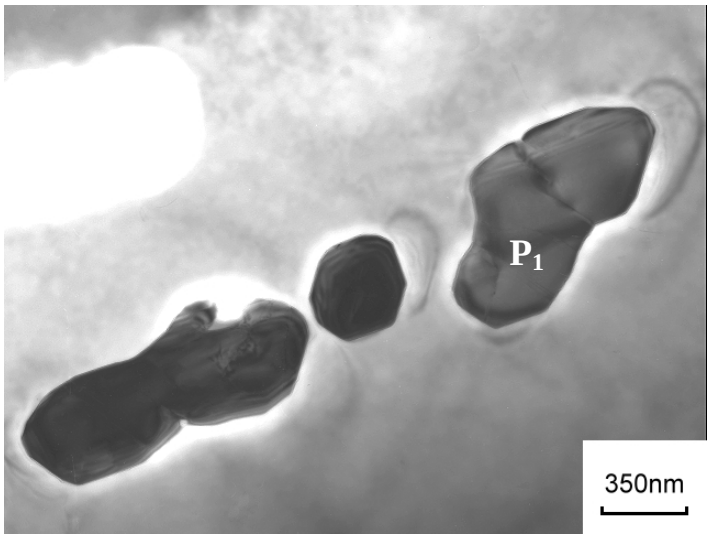

Figure 2(h)

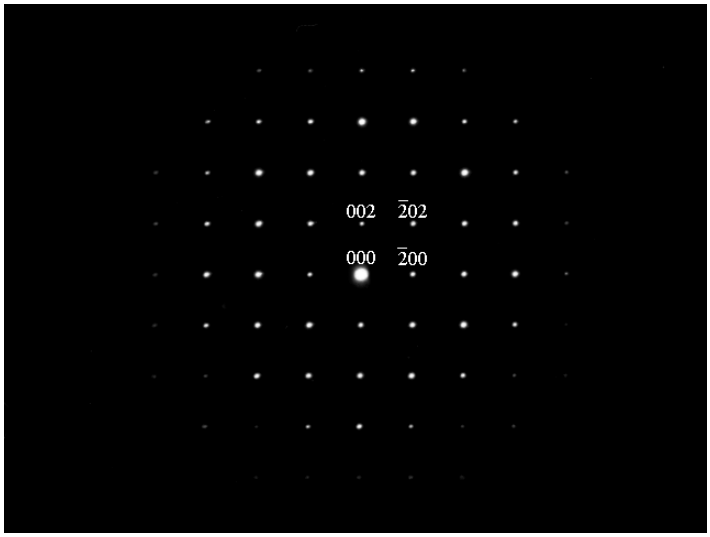

Figure 2(i)

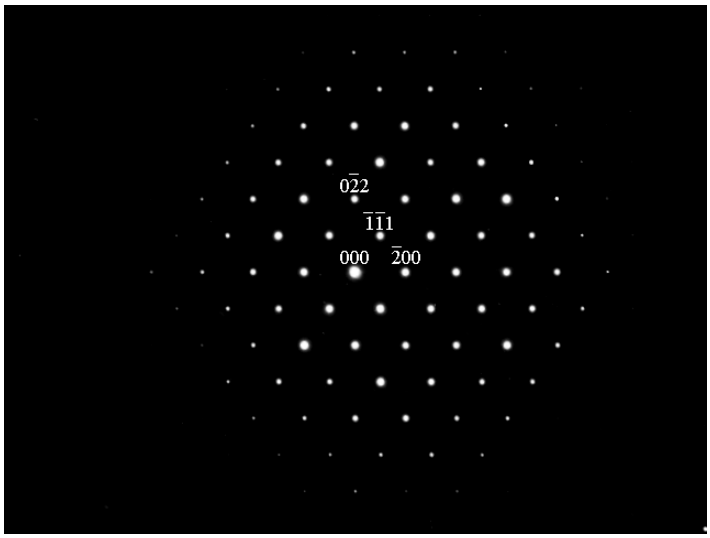

Figure 2(j)

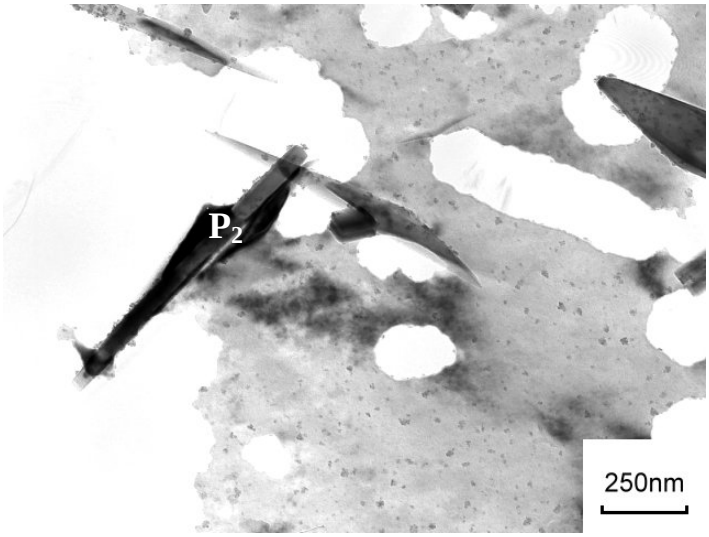

Figure 2(k)

Fig.2 (a) through (c) three SEM micrographs of the alloy aged at 650℃ for 30 minutes. (d) an SADP taken from the grain marked as “A” in (c). The foil normal is [110]. (e) BF, (f) an SADP taken from the grain marked as “F” in (c). The foil normal is [110]. (hkl = ferrite matrix ; hkl = $D0_3$). (g) ($\bar{1}11$) $D0_3$ DF. (h) BF, (i) and (j) two SADPs taken from the precipitate on the grain boundary marked as “P_1” in (c). The foil normals are [010] and [011], respectively. (k) BF taken from the fine precipitate in the ferrite matrix marked as “P_2” in (c).

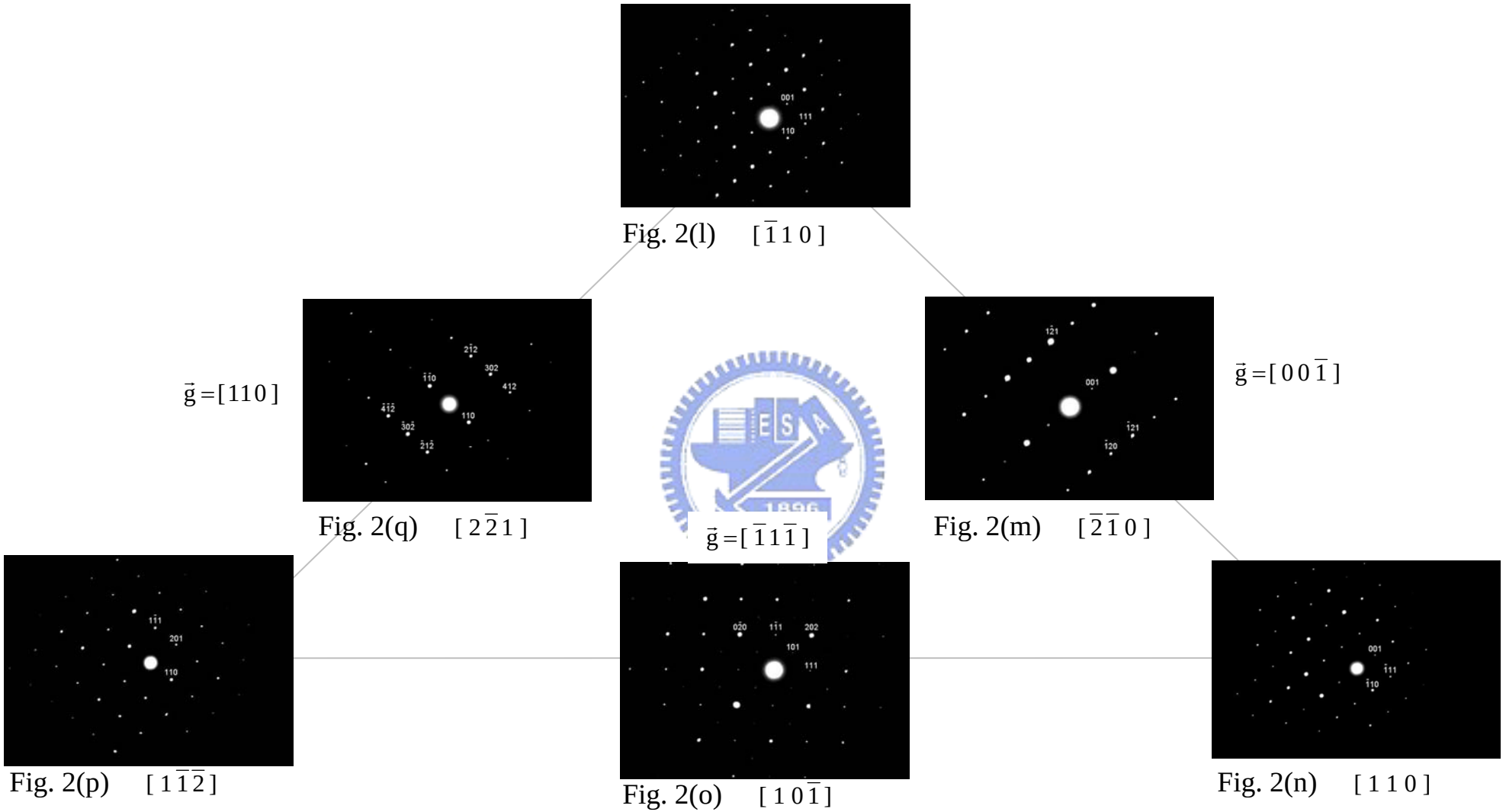

Fig.2 (l) through (q) are six SADPs taken from the fine precipitate in the ferrite matrix marked as "P_2" in Figure 2(c)

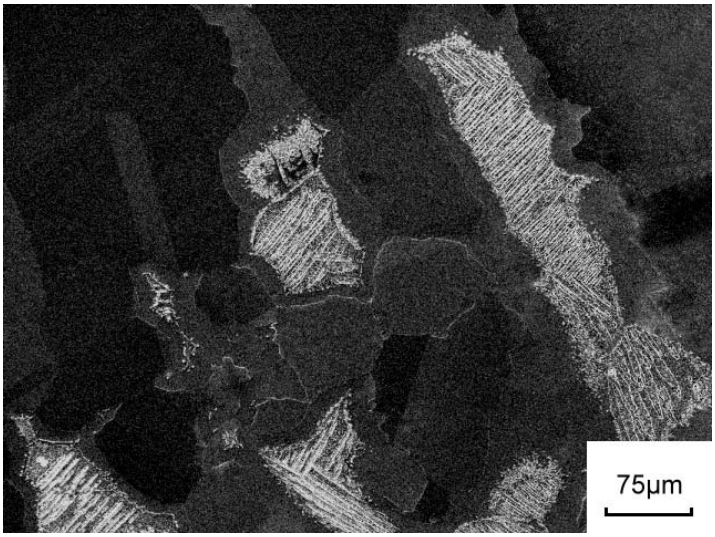

Figure 3(a)

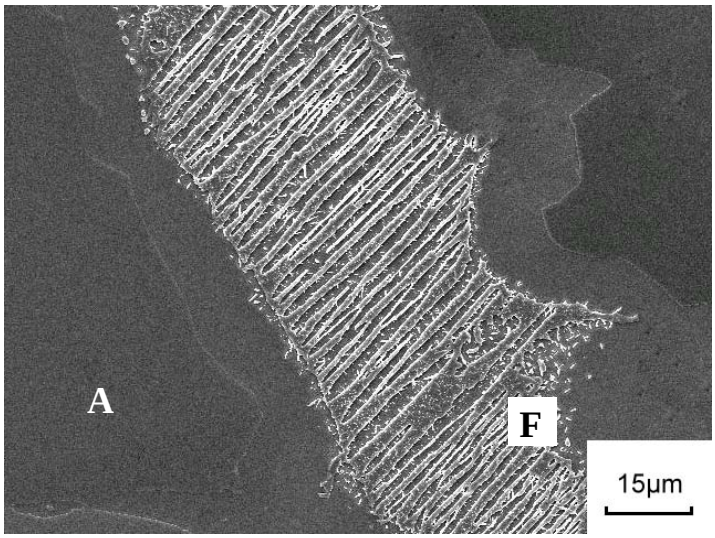

Figure 3(b)

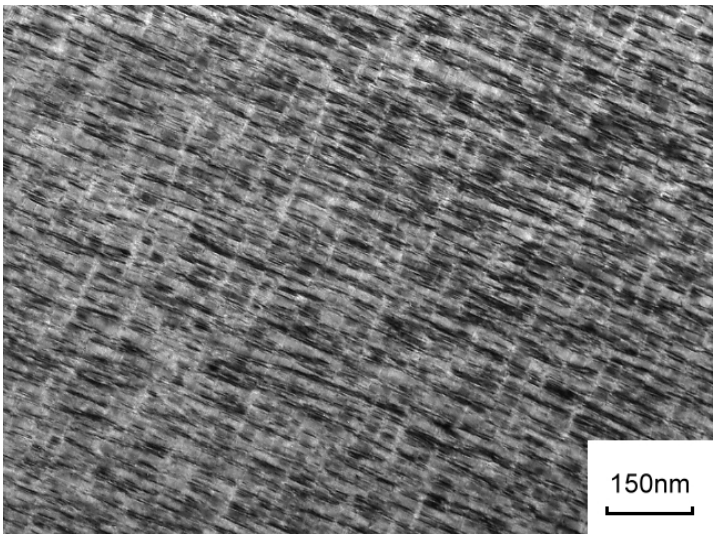

Figure 3(c)

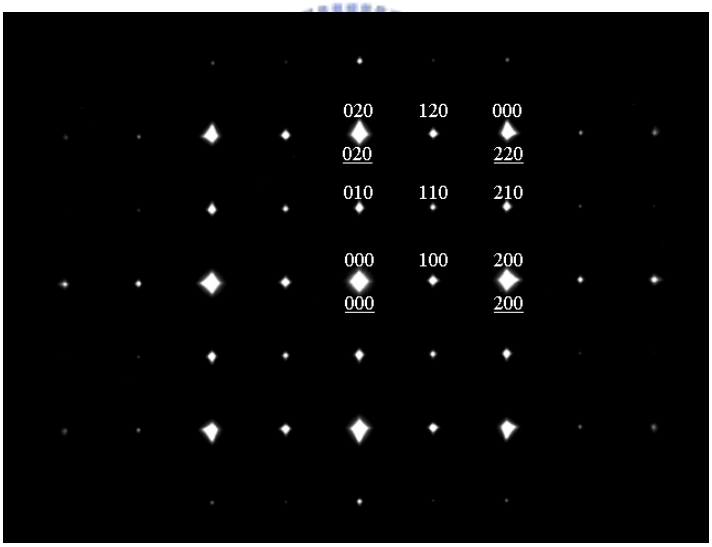

Figure 3(d)

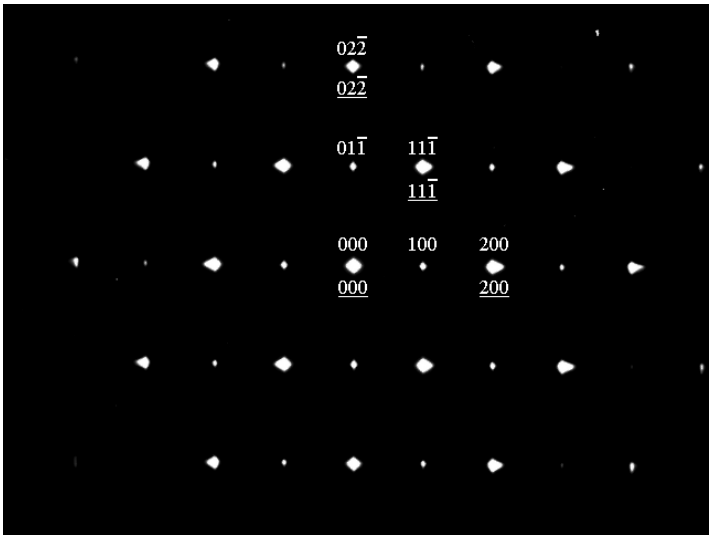

Figure 3(e)

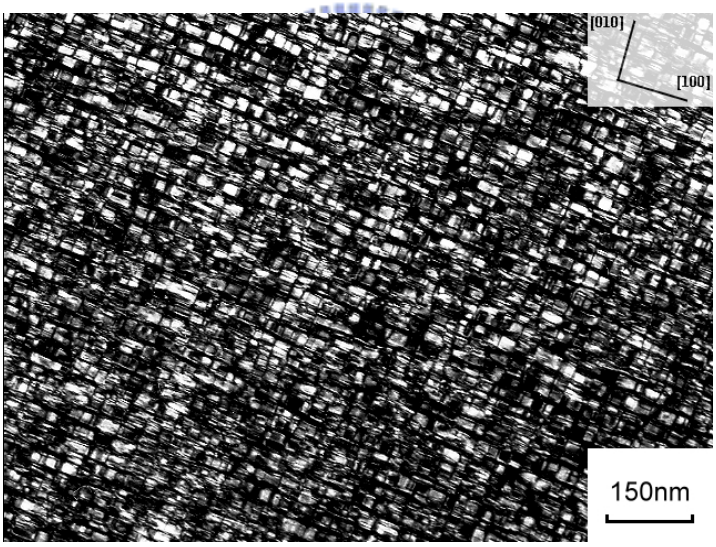

Figure 3(f)

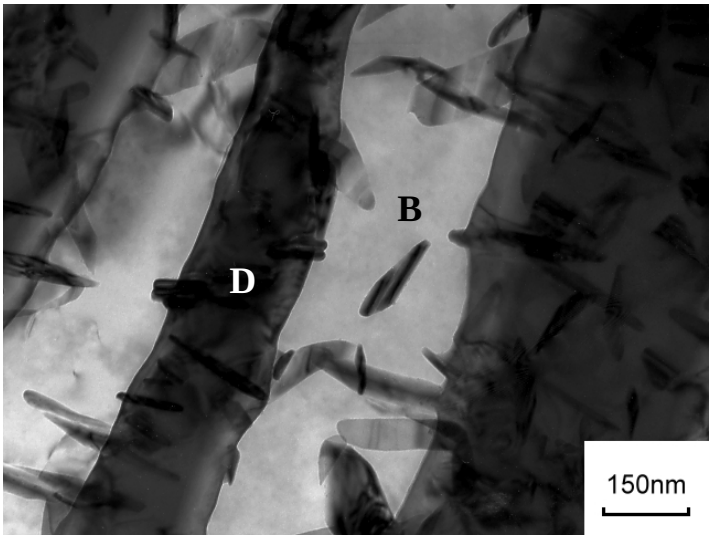

Figure 3(g)

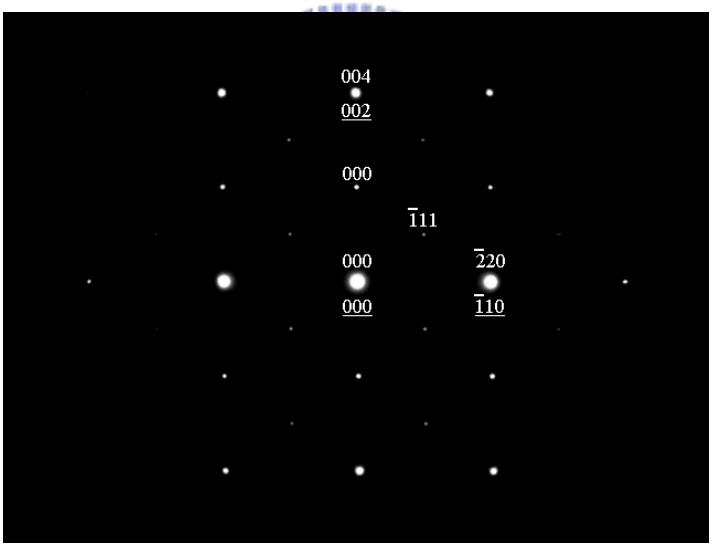

Figure 3(h)

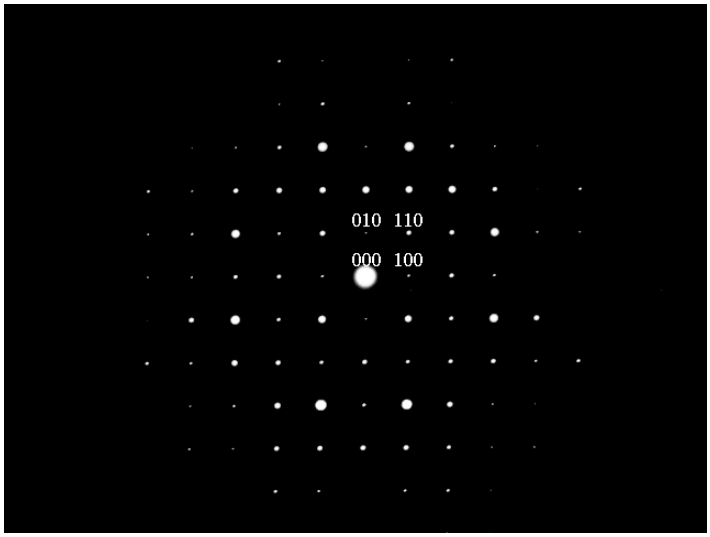

Figure 3(i)

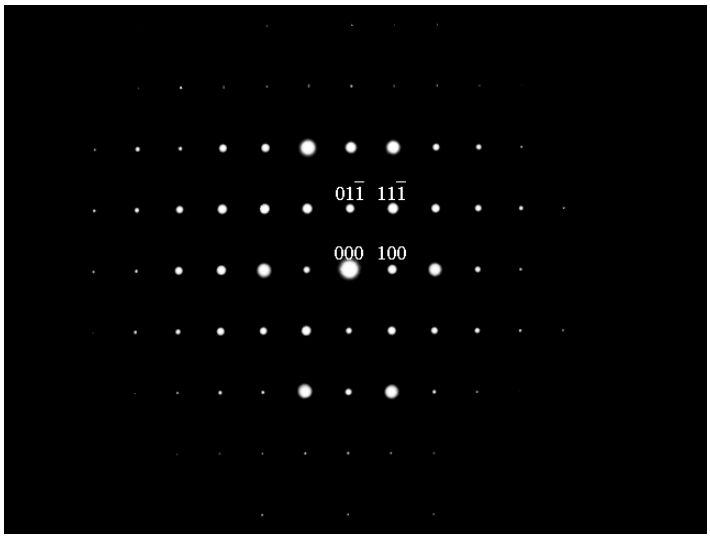

Figure 3(j)

Fig.3 (a) and (b) two SEM micrographs of the alloy aged at 650℃ for 24 hours. (c) BF, (d) and (e) two SADPs taken from the grain marked as “A” in (b). The foil normals are [001] and [011], respectively. (hkl = austenite matrix ； hkl = κ' carbide). (f) (100)

κ' carbide DF. (g) BF, (h) an SADP taken from the ferrite matrix marked as “D” in (g). The foil normal is [110]. (i) and (j) two SADPs taken from the ferrite matrix marked as “B” in (g). The foil normals are [001] and [011], respectively.

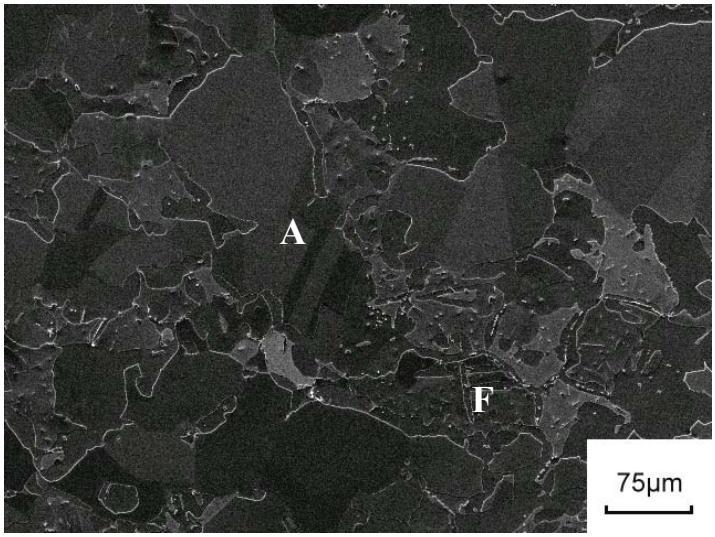

Figure 4(a)

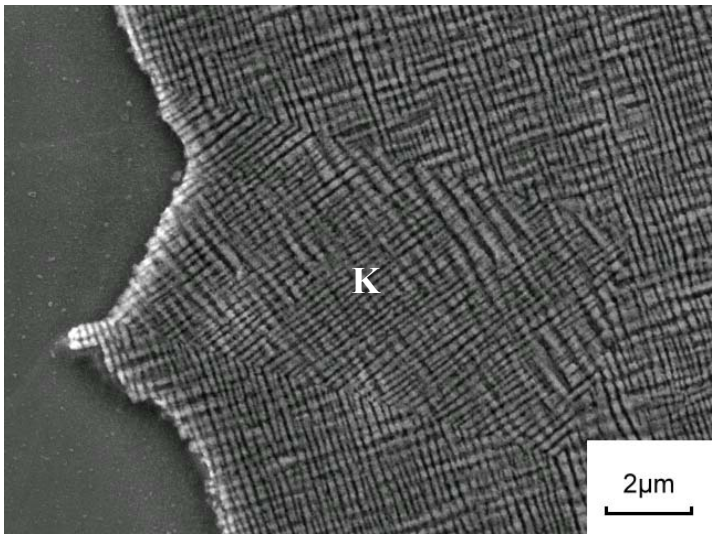

Figure 4(b)

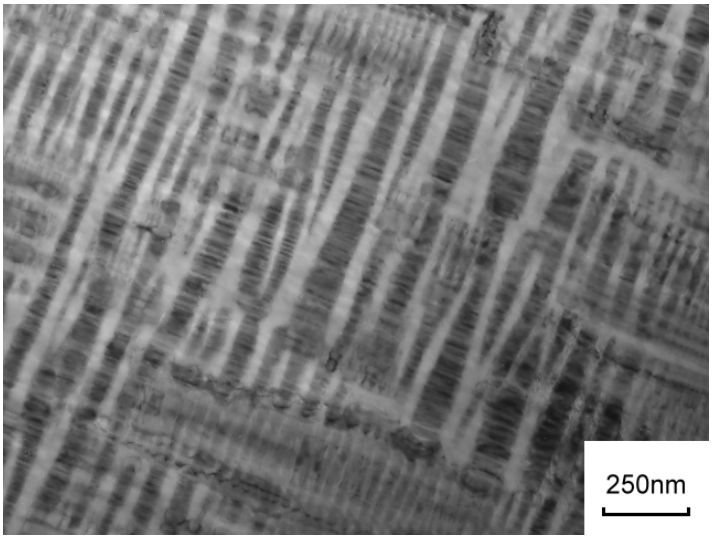

Figure 4(c)

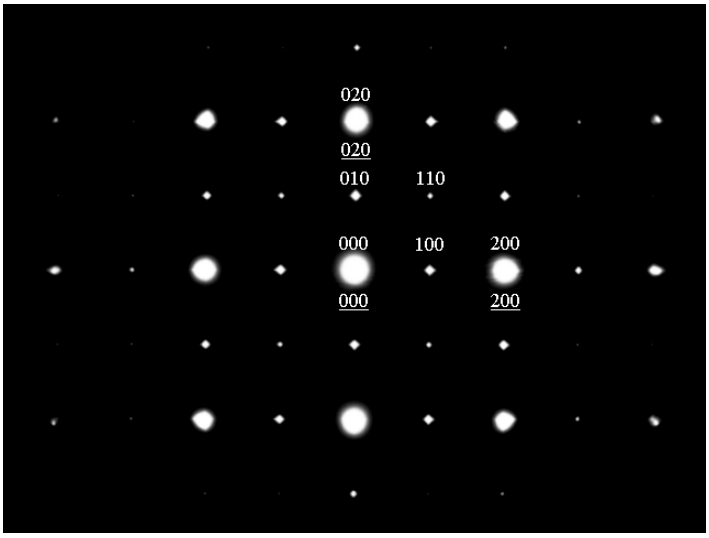

Figure 4(d)

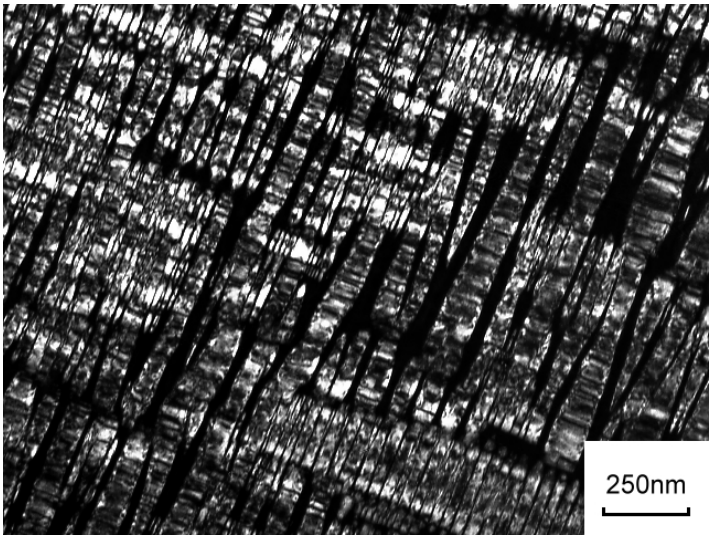

Figure 4(e)

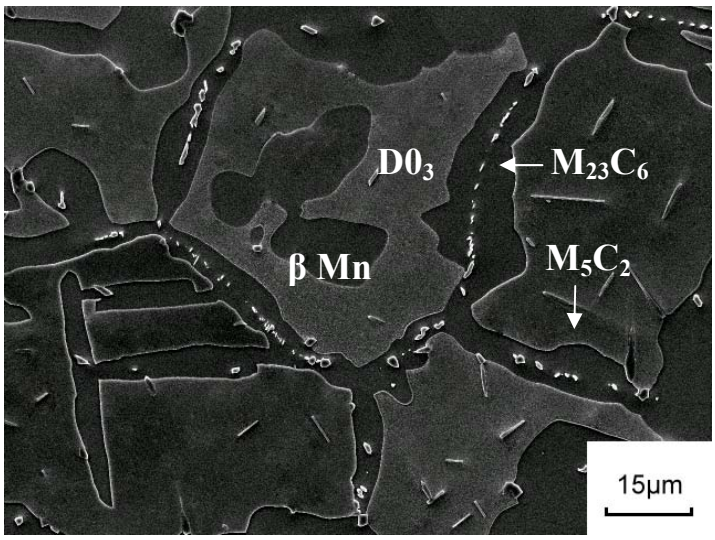

Figure 4(f)

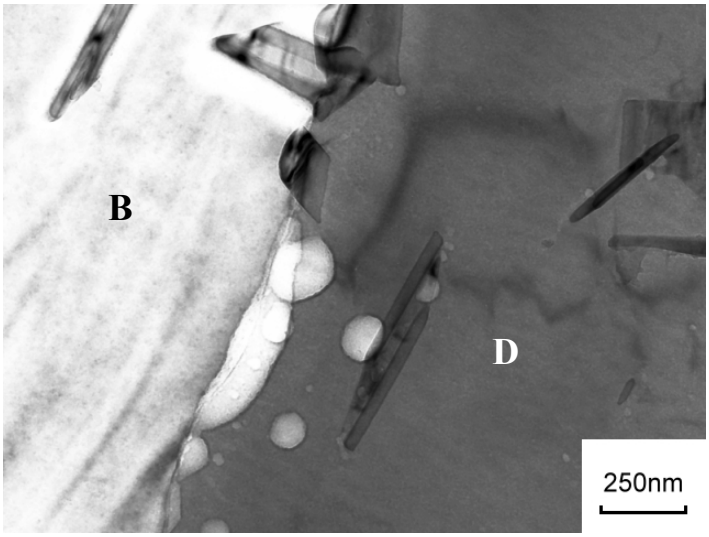

Figure 4(g)

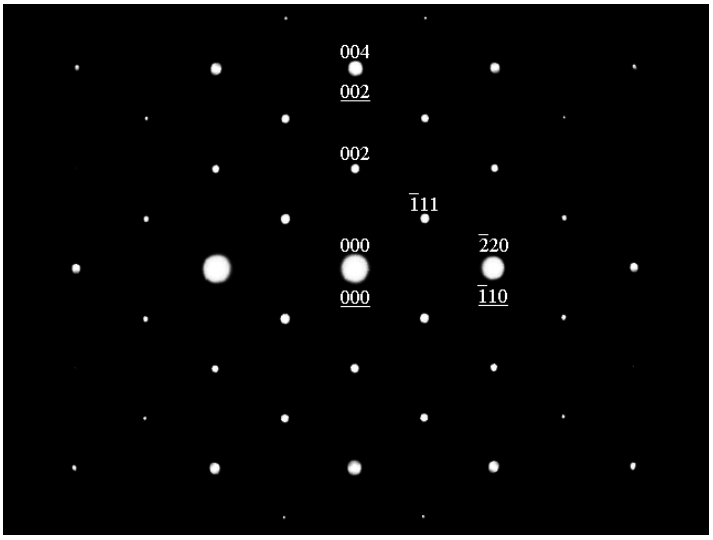

Figure 4(h)

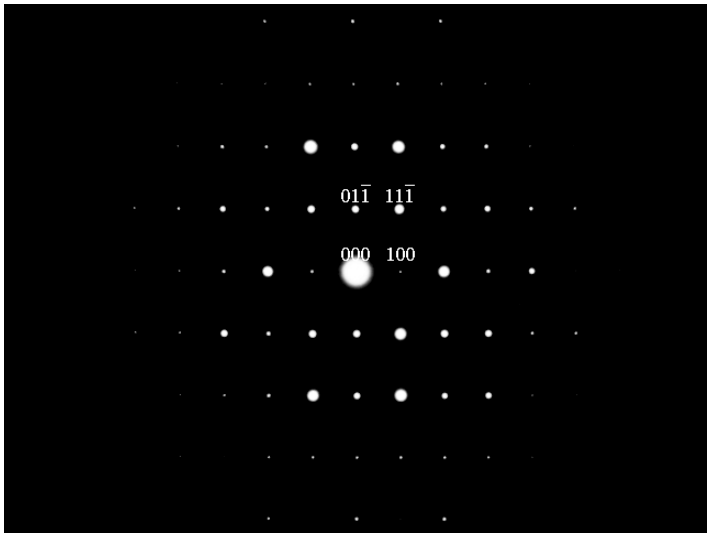

Figure 4(i)

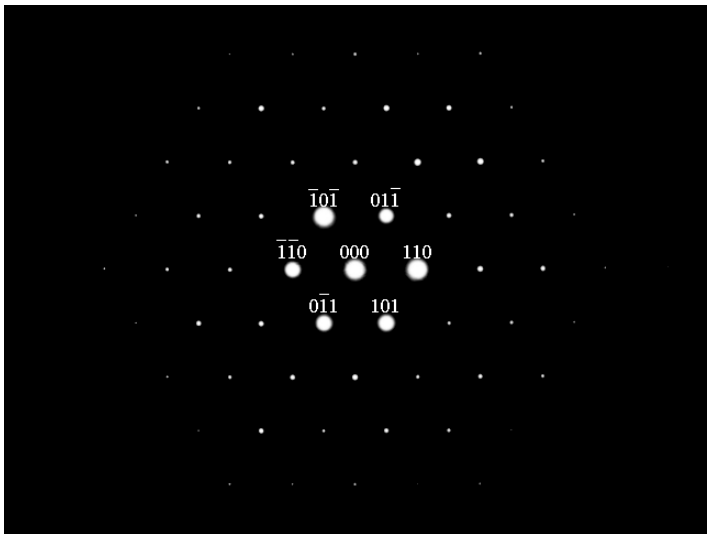

Figure 4(j)

Fig.4 (a) an SEM micrograph of the alloy aged at 650℃ for 7 days. (b) SEM, (c)BF, (d) an SADP taken from the austenite matrix marked as A in (a). The foil normal is [001]. (hkl = austenite matrix；hkl = κ' carbide). (e) (100) κ' carbide DF. (f) SEM, (g) BF electron

micrograph taken from the grain marked as “F” in (a). (h) an SADP taken from the ferrite matrix marked as “$D0_3$” in (f). The foil normal are [011]. (i) and (j) two SADPs taken from the grain marked as “β Mn” in (f). The foil normals are [011] and [$\bar{1}$11], respectively.